

# Retrieval of deformed sea ice area in the southern Sea of Okhotsk using satellite L-band SAR images

Takenobu Toyota<sup>1</sup> and Junno Ishiyama<sup>2</sup>

<sup>1</sup>*Institute of Low Temperature Science, Hokkaido University*

<sup>2</sup>*Toma Town Office, Hokkaido, Japan*

**Introduction:** To improve our understanding of the deformation processes of sea ice, monitoring the temporal evolution of deformed ice area is quite important. For this purpose, SAR is expected to be a useful tool because of its high spatial resolution. While C-band SAR has been used most frequently for the polar sea ice research, it was pointed out that L-band SAR is more suitable for discriminating ridges from level ice than C-band SAR from the comparative analysis of SAR images (e.g., Dierking and Busche, 2006). However, the difference between L-band and C-band SAR in the wide range of the Sea of Okhotsk has not been fully investigated yet, and moreover, in the previous studies for the polar sea ice, validation from the in-situ observation was insufficient. Since in-situ observations have been conducted in the southern Sea of Okhotsk using PV “Soya” every winter in collaboration with Japan Coast Guard, we have available datasets for validation. The purpose of this study is to examine the validity of L-band SAR for detecting the deformed ice area by comparing with a C-band SAR image in the southern Sea of Okhotsk, to develop an algorithm to extract deformed ice area, and then to find the properties of deformed ice area to clarify the dynamical thickening processes in the seasonal ice zone.

**Data:** PALSAR images obtained at a ScanSAR mode in the southern Sea of Okhotsk in January, February, and March from 2009 to 2011 were used in this study. The total number of the images amounted to 35. For comparison, a Radarsat-2 image obtained nearly at the same time was used. The photos and ice thickness data obtained on board the PV “Soya” were used for validation. PALSAR-2 images at a ScanSAR mode were also used to see the applicability of our algorithm.

**Analytical methods:** In analysis, we took four steps as follows: 1) to develop an algorithm to detect deformed ice with L-band SAR, based on in-situ observations, 2) compare between L-band and C-band SARs, 3) map deformed ice area with PALSAR images, and 4) examine the applicability of this algorithm to PALSAR-2 images. With photos, sea ice was categorized into three ice types: nilas (thin level ice), pancake (thin ice with rough surface), and deformed ice (thick ice with rough surface).

**Results:** To develop an algorithm, the backscatter coefficients of PALSAR images were plotted as a function of incidence angle. As a result, the following two threshold curves were derived by the least square method to classify into three ice types.

$$\sigma^0 = -6.0 \log \theta_i + 6.8 \text{ (dB)} \text{ (deformed - pancake ice)} \quad \text{for } 20 < \theta_i < 40 \text{ deg.}$$

$$\sigma^0 = -6.1 \log \theta_i + 3.2 \text{ (dB)} \text{ (pancake ice - nilas)} \quad \text{for } 20 < \theta_i < 40 \text{ deg.}$$

where  $\sigma^0$  and  $\theta_i$  denote a backscatter coefficient and the incidence angle, respectively. In the comparative analysis between Radarsat-2 and PALSAR images, ice types were determined by these thresholds. The results show that 1) L-band SAR is more suitable for detecting deformed ice than C-band SAR also in the southern Sea of Okhotsk, 2) the deformed ice area appears in relatively linear alignments mainly near the ice edge and with a width of a few tens of kilometers in the interior region (Fig.1), 3) affected by winds, ocean waves, and floe interaction, deformed ice area is quite variable with time and space, and 4) when applied to ALOS-2/PALSAR-2 images for the same region in February 2018, reasonable results were obtained. To quantify these properties, further studies are needed.

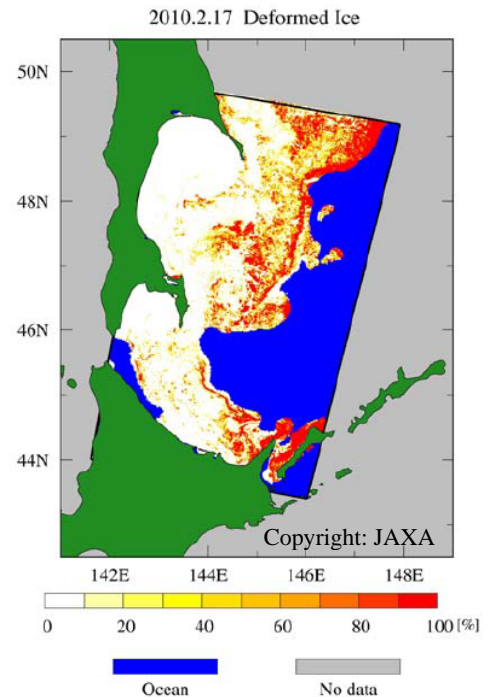


Fig.1 One example of extracted deformed ice area.

## References

Dierking, W. and T. Busch, Sea ice monitoring by L-band SAR: An assessment based on literature and comparisons of JERS-1 and ERS-1 imagery, IEEE Trans. Geosci. Remote Sens., 44(2), 957-970, 2006.